Double-diffusive laminar natural convection in a symmetrical trapezoidal enclosure

Mohamed A. Teamah
Mechanical Eng. Dept., Faculty of Eng., Alexandria University, Alexandria, Egypt
E-mail "mteamah@yahoo.com"

The objective of the present investigation is to study the laminar natural heat and mass transfer in a symmetrical trapezoidal enclosure. The base and ceiling are isothermal and isoconcentration surfaces, while the lateral walls are considered adiabatic and impermeable. A mathematical model is constructed and solved numerically. Both aiding and opposing buoyancy forces have been studied. The investigation is made for wide range of buoyancy ratio N, $-1 \le N \le 10$, inclination angle φ, $0^o \le \varphi \le 18.44^o$, Lewis number Le, $1 \le Le \le 5$ and thermal Grashof number Gr_T, $2x10^3 < Gr_T < 5x10^6$ with fixed aspect ratio A, at A=3, and Prandtl number Pr, at Pr=0.7. The effect of *Le*, N and Gr_T on both local and average Nu and Sh are studied as well as the average Nusselt and Sherwood numbers are correlated in terms of buoyancy ratio and Lewis number. A comparison is made with the previous experimental and numerical results. The comparison shows a maximum deviation from –5% to +12.8%.

البحث يحتوى على دراسه عددية للحمل الرقائقى الحر ثنائى الانتشار (انتقال الحرارة والكتلة) فى حيز على شكل شبه منحرف متماثل لاستخدام هذا الشكل فى العديد من التطبيقات الهندسية كالتقطير الشمسى والبيوت الخضراء وتكييف الهواء، وقد فرض ثبات درجة الحرارة والتركيز لكل من ارضية وسقف الحيز بينما الجدران الرأسية معزولة حراريا وغير نفاذة. وقد تم استنباط نموذج رياضى وتم حلة عدديا، وقد تم دراسة كل من حالة اتحاد وتضاد اتجاة قوي الطفو وقد غطى هذا البحث مدى واسعا للنسبة بين قوتى الطفومن –١ الى ١٠ ورقم جراشوف الحرارى من ٢×١٠^{٣} الى ٥×١٠^{٦} ورقم لويس من ١ الى ٥ وزاوية ميل سقف الحيز من صفر (حيز مستطيل) الى ١٨،٤٤ درجة (حيز مثلث) بينما اجرى البحث عند قيمة ثابتة لرقم براندل عند٠,٧١ عندما تكون النسبة بين نصف طول القاعدة والارتفاع الاقصى للحيز ٣ والذى تم اختيارة فى البحث، وقد تم دراسة تأثير النسبه بين قوة الطفو ورقم لويس وزاوية الميل على كل من خطوط السريان وخطوط ثبات درجة الحرارة وثبات التركيزداخل الحيز وتأثيرهم ايضا على كل من رقم نوسلت ورقم شيروود الموضعى والمتوسط وقد عقدت مقارنة مع الابحاث السابقة وقد اظهرت المقارنة توافق مقبول مع الابحاث النشورة.

Keywords: Double diffusion, Heat and mass transfer, Laminar, Natural convection, Trapezoidal enclosure

1. Introduction

Natural convection in enclosed spaces of various forms occupies a large portion of heat transfer literature. The square, rectangle and cylindrical cavities geometry have been considered in many researches. A few numbers of studies have considered the trapezoidal geometry, which is encountered in several practical engineering applications, such as greenhouses, sun drying crops, water desalination plants and attic spaces in buildings.

Early studies of the combined heat and mass transfer in rectangular enclosures were reported by Hu and EL-Wakil [1], Ostrach [2- 4] and Lee et al. [5]. Bejan et al. [6, 7] conducted an analytical and numerical study of the combined heat and mass transfer in a vertical rectangular enclosure with uniform heat and mass fluxes along the vertical sides. They studied the effect of Lewis number by using a similarity solution. Viskanta et al. [8] examined the effect of combined lateral temperature and concentration gradients on natural convection in a two-dimensional square cavity filled with a binary gas. Numerical work on double-diffusive natural convection in a square cavity was more reported by Beghein et al. [9]. They correlated the heat and mass transfer rate in terms of Lewis, solutal Rayleigh and Schmidt numbers for heat or mass driven flows. Han and Kuehn [10, 11] studied experimentally and numerically the double-diffusive natural convection in a vertical rectangular enclosure. They presented a flow map showing the single and multi cell

regions as a function of Lewis number and buoyancy ratio.

Natural convection in trapezoidal enclosures have been presented by Poulikakos and Bejan [12], and Lam et al. [13]. Lee [14] studied natural convection in tilted nonrectangular enclosure numerically and experimentally. Salmun [15] studied the convective patterns in a triangle domain. Voropoulos et al. studied the trapezoidal geometry in the distillation of saline water in greenhouse type solar stills [16]. Few researchers have presented results on the associated flow and heat transfer problem, considering either symmetric as Rheinllnder [17] and Palacio et al. [18] or single-slope still geometries as studied by Djebedjian and Abou Rayan [l9]. Papanicolaou et al. [20] have presented numerical results for the flow and temperature fields in an asymmetric greenhouse-type solar still and explain the effect of physical and geometric parameters. Boussaid et al. [21] studied numerically the laminar-flow regime in an enclosure with a single inclined surface at the top. They studied various angles of inclination and Lewis numbers. The binary fluid was air/water vapor and numerical results were obtained for assisting buoyancy forces, the majority of which was at N= 1. For thermal Rayleigh numbers (based on height) Ra > 2x 10^5.

The interesting phenomena occur when the two buoyancy forces, i.e., those due to thermal and solutal effects, oppose each other and the buoyancy ratio is negative. Such configurations, where the driving temperature and concentration gradients may be applied either in the horizontal or in the vertical direction, are prone to instabilities and bifurcation phenomena. Ghorayeb et al. [22 and 23], have presented comprehensive results as for as the nature of the bifurcations and the respective critical values for their onset. The influence of the aspect ratio, Lewis number and angle of inclination have been investigated. However, oscillatory phenomena have been observed also for vertically imposed gradients in rectangular geometries by Mamou et al. [24]. Recently Papanicolaou and Bekssiotis [25] studied turbulent natural convective heat and mass transfer in an asymmetric trapezoidal enclosure in the two dimensions numerically. They studied both aiding and opposing buoyancy forces $-1<N\leq 1$. Their solutions yield a multi-cellular flow field, with the number of cells depending on the Rayleigh number for a fixed Lewis number and geometry.

From the previous review, the effect of inclination angle of the symmetrical trapezoidal enclosures as well as the effect of Lewis number and the buoyancy ratio had a shortage of the predicted results and correlations to calculate the rate of heat transfer and mass transfer. Therefore, this research devoted to study these effects for a wide range for Lewis number and buoyancy ratio. The obtained results for average Nusselt and Sherwood numbers were correlated.

2. Mathematical formulation

Fig. 1 shows a schematic of the problem considered. A symmetric trapezoidal enclosure with flat horizontal base with length 2L, and inclined ceiling with an angle φ to the horizontals. The bottom and ceiling surfaces are considered isothermal and isoconcentration, while the vertical walls are considered adiabatic and impermeable. Qualitative description of the flow directions for both aiding and opposing buoyancy ratios were discussed by Papanicolaou et al. [20]. The flow in the cavity is considered to be steady and two-dimensional. Neglecting heat transfer by radiation and the fluid is assumed Newtonian and nearly incompressible and the viscous dissipation is neglected. By introducing the above assumptions into the conservation equations of mass, momentum, energy, and mass species in the Cartesian coordinates, using the Boussinsq approximation for the buoyancy term in the momentum equation given as;

$$\rho = \rho_o \left[1 - \beta_T (T - T_o) - \beta_S (c - c_o) \right]. \qquad (1)$$

And then introducing the following dimensionless groups for the governing equations,

$$X=\frac{x}{H_o}\ ,\ Y=\frac{y}{H_o},\ U=\frac{u\,H_o}{\alpha}\ ,V=\frac{v\,H_o}{\alpha}\ ,P=\frac{p\,{H_o}^2}{\rho_o * \alpha^2},$$

$$\theta=\frac{T-T_o}{T_i-T_o}\ \text{and}\ C=\frac{c-c_o}{c_i-c_o}, \tag{2}$$

a set of governing equations is obtained as:

$$\frac{\partial U}{\partial X}+\frac{\partial V}{\partial Y}=0\,. \tag{3}$$

$$U\frac{\partial U}{\partial X}+V\frac{\partial U}{\partial Y}=-\frac{\partial P}{\partial X}+Pr\left[\frac{\partial^2 U}{\partial X^2}+\frac{\partial^2 U}{\partial Y^2}\right]. \tag{4}$$

$$U\frac{\partial V}{\partial X}+V\frac{\partial V}{\partial Y}=-\frac{\partial P}{\partial Y}+Pr\left[\frac{\partial^2 V}{\partial X^2}+\frac{\partial^2 V}{\partial Y^2}\right]+Ra_T\,Pr\left[\theta+NC\right]. \tag{5}$$

$$U\frac{\partial \theta}{\partial X}+V\frac{\partial \theta}{\partial Y}=\left[\frac{\partial^2 \theta}{\partial X^2}+\frac{\partial^2 \theta}{\partial Y^2}\right]. \tag{6}$$

$$U\frac{\partial C}{\partial X}+V\frac{\partial C}{\partial Y}=\frac{1}{Le}\left[\frac{\partial^2 C}{\partial X^2}+\frac{\partial^2 C}{\partial Y^2}\right]. \tag{7}$$

With the boundary conditions:

At Y=0, U=V=0, and θ=C=1. (8)

At Y= H_x/H_o, height of the top inclined ceiling, U=V=θ=C=0. (9)

At X= -A, and at X=A:

$$U=V=\frac{\partial \theta}{\partial X}=\frac{\partial C}{\partial X}=0\,. \tag{10}$$

2.1. Nusselt number calculation

Equating the heat transfer by convection to the heat transfer by conduction at the bottom of the cavity gives:

$$h\ \Delta T=-K\left(\frac{\partial T}{\partial y}\right)_{y=0}\ . \tag{11}$$

Introducing the dimensionless variables, defined in eq. (2), into eq. (11), gives:

$$Nu_i=-\left(\frac{\partial \theta}{\partial Y}\right)_{Y=0}\ . \tag{12}$$

The average Nusselt number is obtained by integrating the above local Nusselt number over the base surface:

$$Nu=-\frac{1}{2A}\int_{-A}^{A}\left(\frac{\partial \theta}{\partial Y}\right)_{Y=0}dX\,. \tag{13}$$

2.2. Sherwood number calculation

Equating the extracted mass transfer by convection to the added mass transfer to the cavity gives:

$$h_s\Delta c=-D\left(\frac{\partial c}{\partial y}\right)_{y=0}\ . \tag{14}$$

Introducing the dimensionless variables, defined in eq. (2), into eq. (14), gives:

$$Sh_i=-\left(\frac{\partial C}{\partial Y}\right)_{Y=0}\,. \tag{15}$$

The average Sherwood number is obtained by integrating the above local Sherwood number over the base surface:

$$Sh=-\frac{1}{2A}\int_{-A}^{A}\left(\frac{\partial C}{\partial Y}\right)_{Y=0}dX\ . \tag{16}$$

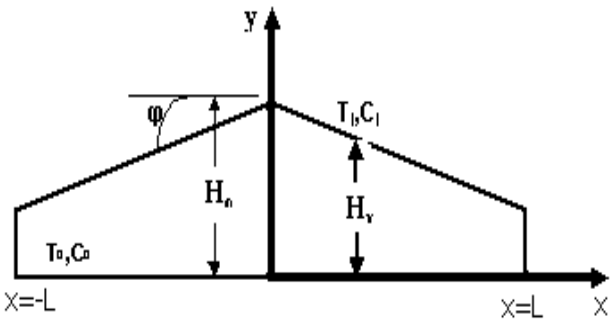

Fig. 1. Geometry of the trapezoidal cavity with boundary conditions.

3. Solution proccedure

The cavity is symmetric about the centerline, Y-axis. Therefore, only the right half was solved by introducing the following boundary conditions at X=0.

$$\frac{\partial U}{\partial X} = \frac{\partial V}{\partial X} = \frac{\partial \theta}{\partial X} = \frac{\partial C}{\partial X} = 0 \quad . \tag{17}$$

Firstly, the number of nodes used was checked. Through out this study, the number of grids (84 × 102) was used. The 102-grid points in the vertical direction are enough to resolve the thin boundary layer near both the upper and bottom surfaces sufficiently. Finite volume technique developed by Patankar [26] was used, which is based on the discretization of the governing equations using the central differencing in space. A uniform grid was taken in the horizontal direction. On the other hand non-uniform grid was taken in the vertical direction. The control volume height was fine at the external boundaries with short height and thick at the cavity center to achieve the angle of inclination. The ratio between the heights of the control volume at outer boundaries and at center of the cavity depended on ceiling inclination angle. Fig. 2 shows a sample for grid lines and control volumes. The discretization equations were solved by the Gauss-seidel method. The iteration method used in this program is a line-by-line procedure, which is a combination of the direct method and the resulting Tri Diagonal Matrix Algorithm (TDMA). The accuracy was defined by the change in the average Nusselt number through one hundred iterations to be less than 0.01 % from its value. The check showed that 4000 iterations were enough for all of the investigated values.

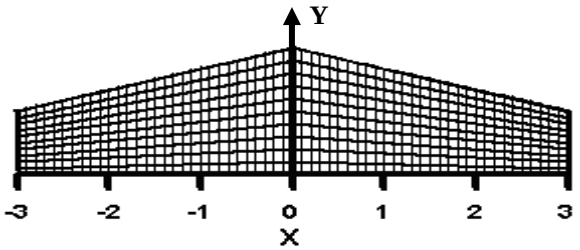

Fig. 2. Geometry of the enclosure with shape of grids in the dimensionless form.

4. Results and discussions

4.1. Hydrodynamic flow results and discussions

In this investigation, the Prandtl number, Pr is kept constant at Pr = 0.7, and aspect ratio, A=3. The base case in this study is made with φ=10°. It is found that, for -1 ≤ N < 0, there is a very weak flow due to competition between two forces opposing each other. The first one is the thermal buoyancy force due to the heat transfer and thermal expansion, which acts to the upward direction. The second one is the buoyancy force, due to the mass transfer, which acts to direction of downward and opposes the thermal force.

Samples of streamlines, isotherms, and isoconcentration are shown in figs. 3 to 5. Fig. 3 represents the streamlines, and isotherms when Le=1 with different N. For Lewis number equals one, the isothermal lines distributions are congruent with the isoconcentration lines. Therefore, the isothermal lines are enough to show the distribution of both isothermal and isoconcentration lines. For N=0. Fig. 3-a, as an example, it is observed that, the flow field is characterized by four recirculating cells in each portion of the cavity. As N is increased, the characteristics of the flow field don't change but the flow becomes stronger.

As Le is increased, as shown in fig. 4 for Le=3, and fig. 5 for Le=5, and the value of the thermal Grashof number in the two figures is kept constant, $Gr_T=10^5$. It can be observed the same characteristics when Le=1. As N is increased, for N>1, a transition of the flow field from four cells to three cells in each portion is noticed. With further increase in N, a transition from three cells pattern to two cells pattern in each portion of the cavity is occurred. With further increase of N, the two cells in the middle of the cavity become very weak, and the other two cells in the corners become stronger due to the increasing of the circulation.

The effect of the inclination angle, φ can be seen in fig. 6 for Le=1, and buoyancy ratio N=1. It is noticed that, for φ = 0° (rectangular cavity), the flow field is characterized by four strong recirculating cells in each portion of the cavity. With increasing the inclination angle φ, it is noticed that, there is a transition of flow

field from four cells to three cells in each portion of the cavity. As seen in fig. 6-e, for maximum inclination angle for the investigated range for aspect ratio A, at A=3 (φ = 18.44°). At this inclination angle the cavity will be triangular cavity. In this cavity, the enclosure is very narrow at the two edges. Therefore a high resistance for recirculating flow occurred. The figure shows, two strong cells at the middle of the cavity followed by four very weak cells, two in each portion of the cavity.

4.2. Heat and mass transfer results and discussion

Samples of the characteristics of isotherms and isoconcentration lines are presented in figs. from 3 to 6. Through these figures, the thermal Grashof number is kept constant and equal to 10^5, while both Lewis number and buoyancy ratio are changed. As shown in fig. 3, for Lewis number *Le*=1, and buoyancy ratio N=1, the isothermal field is characterised by a big upward thermal plume in the middle of the cavity followed by two downwards thermal plumes, one in each portion of the cavity, followed by another two upwards thermal plumes. It is noticed that, there are a transition in direction of the thermal plumes guided by the thermal plume in the middle of the cavity. With increasing N, however, it can be seen that, the thermal plumes are still in their directions, but stratified in some of it and becomes sharp. As Lewis number is increased, figs. 4 and 5, for *Le*=3, and *Le*=5, it can be seen a similar characteristics with those for *Le*=1, when N=0. Conversely, with further increase of buoyancy ratio N, the thermal plumes directions are reversed, and reduced to two plumes, one in each portion of the cavity. However, with further increase of *N*, the thermal plumes directions are reversed again, and are stratified. It is noticed that, the isothermal plumes at high Lewis number, and high buoyancy ratio, are stratified and consist of a stratified plume in the middle of the portion tilted downwards, followed by two stratified plumes, one in each portion of the cavity, tilted upwards. Also, it can be seen from these figures as the Lewis number increases, the isoconcentration lines at the cavity base become closer than the isothermal lines. This is due to the diffusion of mass is higher than the diffusion of heat.

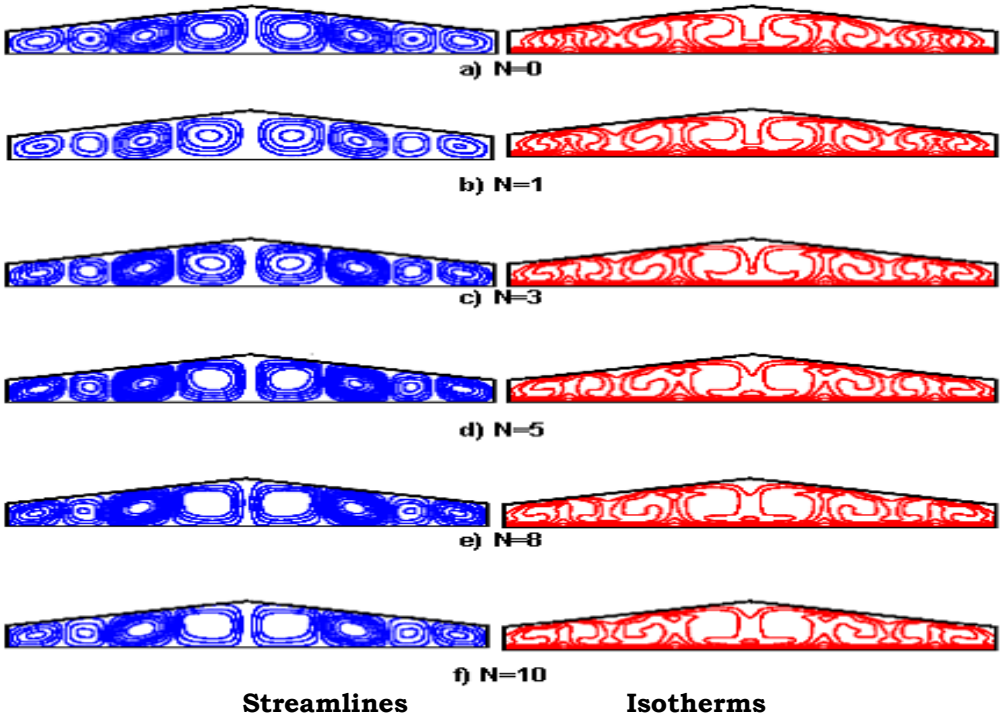

Fig. 3. Streamlines and Isotherms for A=3, *Le*=1, φ=10°, and Gr_T=10^5.

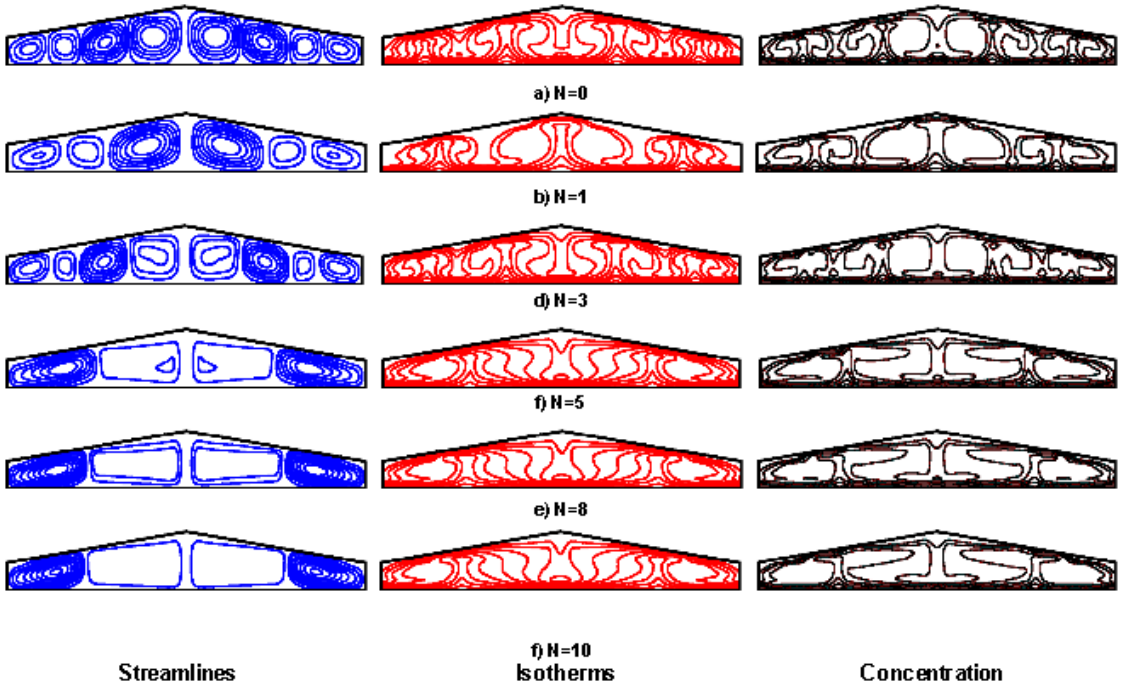

Fig. 4. Streamlines, isotherms, and concentration for A=3, Le=3, φ=10°, and Gr_I=10^5 a) N=0, b) N=1, c) N=3, d) N=5, e) N=8, and f) N=10.

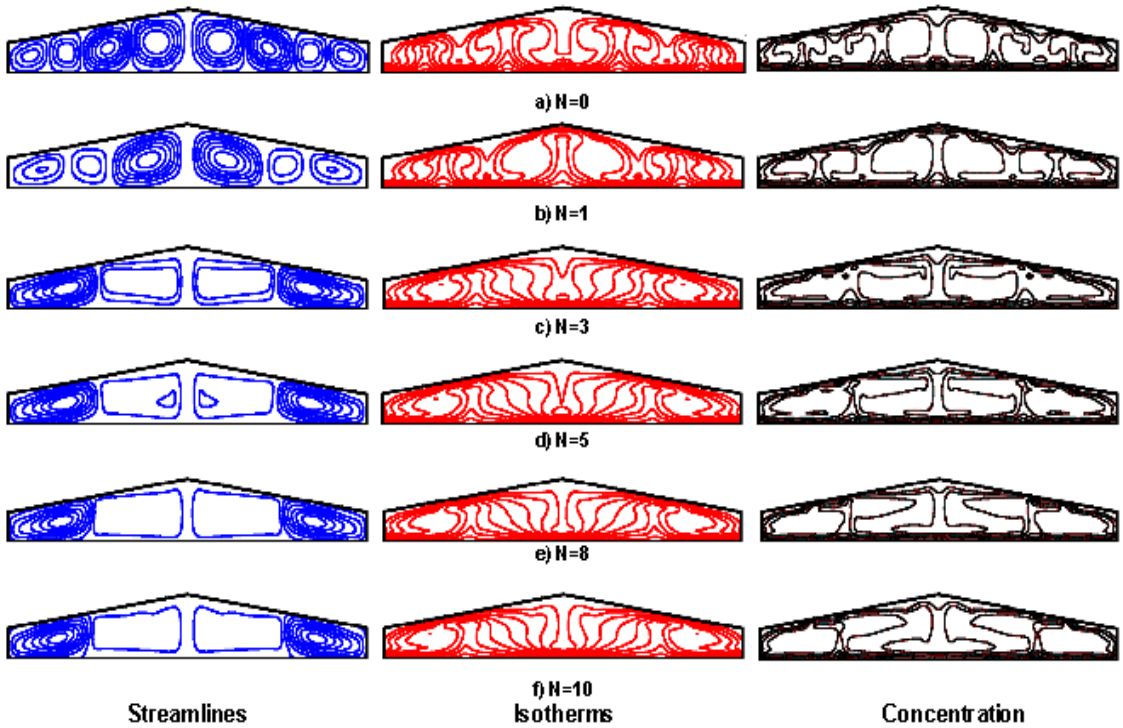

Fig. 5. Streamlines, isotherms, and concentration for A=3, *Le*=5, φ=10°, and Gr_I=10^5, a)N=0, b) N=1, c) N=3, d) N=5, e) N=8, and f) N=10.

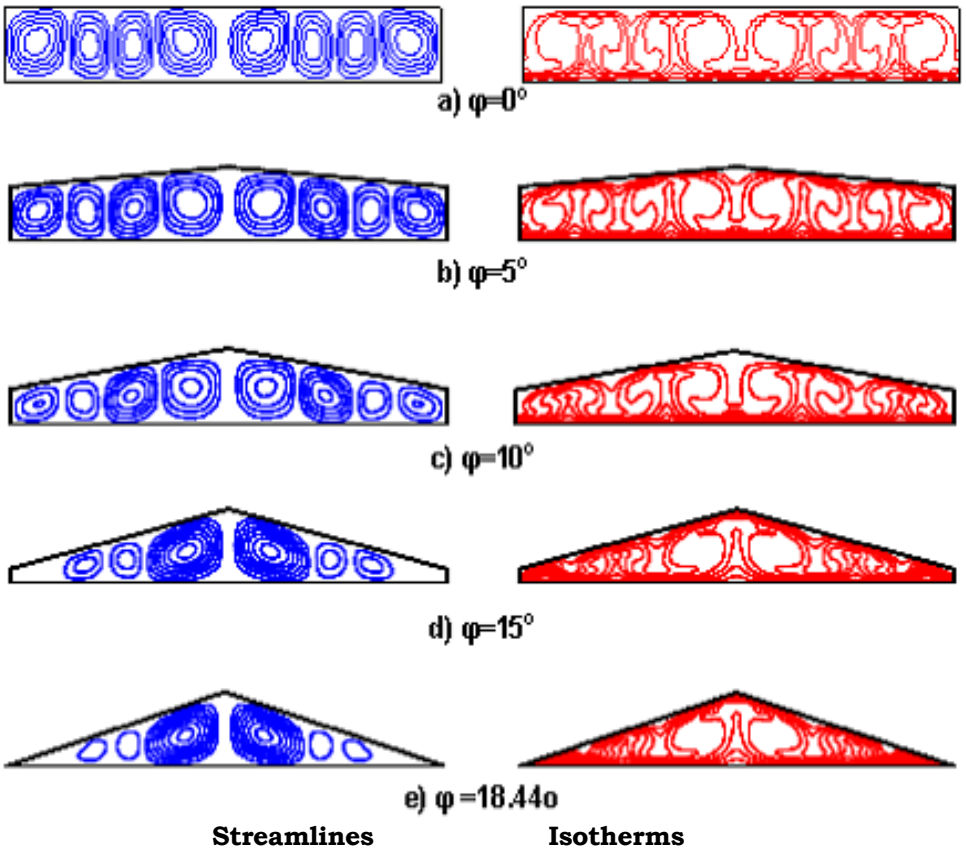

Fig. 6. Effect of inclination angle (φ) on Streamlines, and Isotherms for A=3, Le=1, N=1, and Gr_T=10^5.

Fig. 6 shows the effect of the ceiling inclination angle φ, on the streamlines. As the inclination angle is increased, the streamlines at the corners of the cavity become stratified. At these zones, the conduction is dominated. Therefore, both heat and mass are transferred mainly by conduction in these zones.

Figs. 7 and 8 plot the local Nusselt and Sherwood numbers for different Lewis number respectively. Both local Nusselt and Sherwood look like the saw tooth. This phenomena was observed by Boussaid et al. [21] and Papanicolaou and Belessiotis [25]. Both local Nusselt and Sherwood numbers have peak values when the flow cells are coming towards the cavity base and have minimum values when the flow cells depart from the cavity base. This can be also detected from isothermal and isoconcentration lines. These lines are very close at the positions of the peak values and far apart from each other at the position of minimum local values.

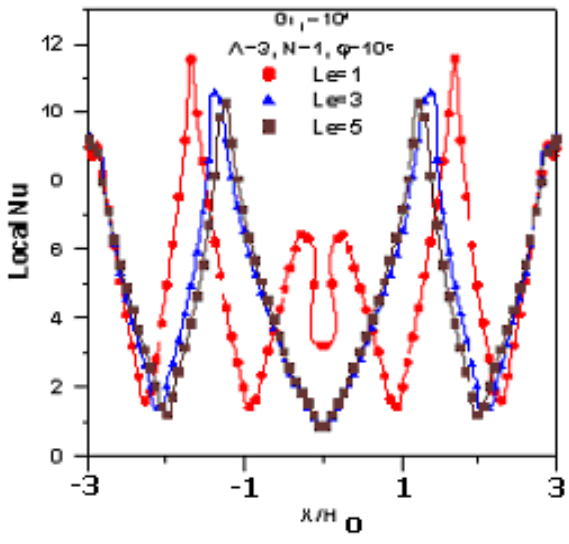

Fig. 7. Effect of Lewis number on local Nusselt number.

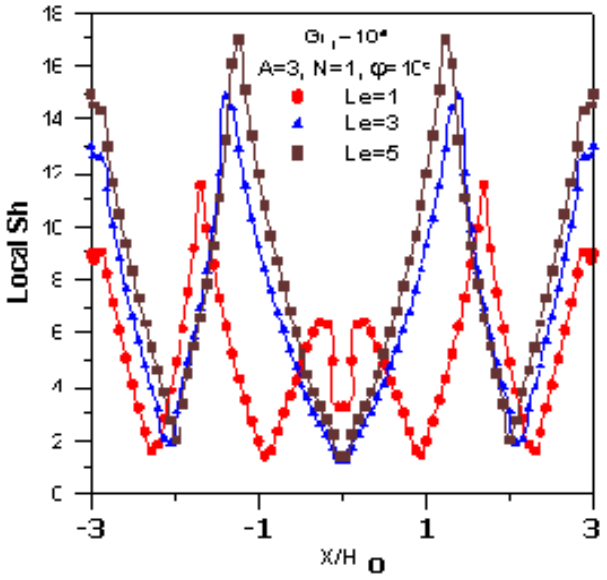

Fig. 8. Effect of Lewis number on local Sherwood number.

The average Nusselt number is calculated by using eq. (13). The relation between the average Nusselt and buoyancy ratio for different Lewis numbers is plotted in fig. 9 for $Gr_T = 10^5$, A =3, and $\varphi = 10^o$. For small buoyancy ratio, $-1 \le N \le 0$, there is no effect of increasing Lewis number on the value of the average Nusselt, so the average Nu has nearly a constant value which depends only on the buoyancy ratio. For $0 < N < 2.0$, the average Nusselt is decreased slowly with the Lewis number. As the effect of the driven force by mass is increased, for $2 < N \le 10$, the circulation of the flow tends to stratify the temperature field. With further increase of N, the average Nusselt is increased for Le=1 due to the increasing of circulation of the flow field which increases the heat transfer. For $3 < N \le 5$, and $Le > 1$, the average Nusselt is decreased rapidly as the buoyancey ratio. After this decrease, the average Nusselt returned to increase with the buoyancy ratio. The rapaid decreasing in average Nu curves is due to the transition of the flow field from four pair of cells to three pair of cells, or a transition from three pair to two pair of cells.

The values of average Nusselt nmber for the investigated range of both Lewis number and buoyancy ratio are correlated as function of N, and Le, in the following forms:

$$Nu = 6.358 N^{0.0294} Le^{-0.188} . \qquad (18)$$

The above correlation is valid for:
$2.0 \le N \le 10$, $2 \le Le \le 5$, and $Gr_T = 10^5$, when A =3, and $\varphi = 10^o$.

The standard deviation for the above correlation is 0.048, and the maximum error within +7%.

A relationship between the average Nusselt number, and the buoyancy ratio for different ceiling inclination angle φ when $Gr_T = 10^5$, A =3, Le = 1 is presented in fig. 10. As it is seen, for small buoyancy ratio, as the buoyancy ratio is increased, the values of the average Nusselt number don't depend on the inclination angle. The average Nusselt number is increased rapidly for $-1 \le N \le 3$ for all investigated φ. However, as the buoyancy ratio is increased, the average Nusselt number increases slightly for high inclination angles. It is also seen that in the investigated range for buoyancy ratio, for $0 \le \varphi < 10^o$, there is a rapid decreas followed by an icrease in the average Nu in the middle of the curves due to the transition of the flow fields. For rectangular cavity with φ equals zero, the transition in the average Nusselt number occurs at buoyancy ratio equals to three. The value of buoyancy ratio at the transition is increased as the ceiling inclination angle is increased.

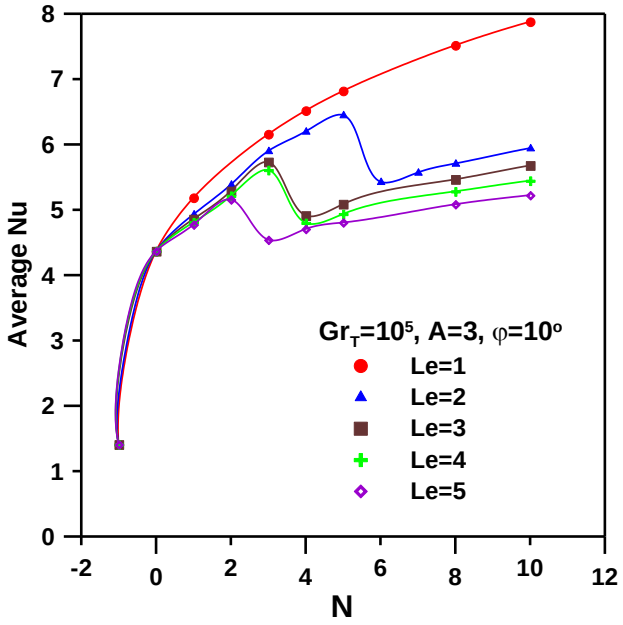

Fig. 9. Average Nu as a function of buoyancy ratio for A=3, $\varphi=10^o$, and $Gr_T=10^5$.

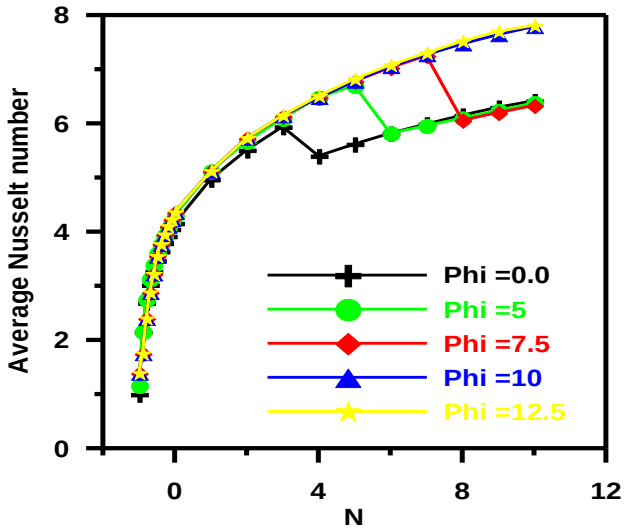

Fig. 10. Average *Nu* as a function of N for A=3, *Le*=1, and Gr_T=10^5.

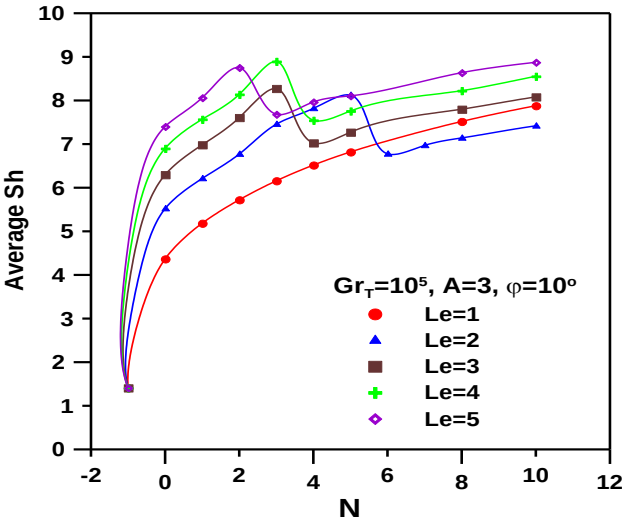

Fig. 11. Average Sh as a function of buoyancy ratio for A=3, φ=10°, and Gr_T=10^5.

The average Sherwood number is calculated by using eq. (16). The relationship between the average Sherwood number and buoyancy ratio for different Lewis number, with A=3, φ = 10°, and Gr_T = 10^5 is plotted in fig. 11. Generally, it is noticed that, as Lewis number is increased, the average Sherwood number is increased due to the diffusion increase with mass transfer except for N = -1, the average Sherwood has a constant value for different values for Le. At this value of buoyancy ratio N=1, the flow is stagnant and both heat and mass are transferred by pure conduction. For N ≥ 3, it can be seen that a rapid decrease in the curves of the average Sherwood number is due to the transition of the flow fields.

The values of the average Sherwood number for the investigated range of both Lewis number and buoyancy ratio were correlated. The correlated result is in the following form:

$$Sh = 6.561N^{0.0227}\,Le^{0.1303}\,. \qquad (19)$$

The above correlation is valid for:
2.0 ≤ N ≤ 10, 2 ≤ *Le* ≤ 5, and Gr_T = 10^5, when A =3, and φ=10°.

The standard deviation for the above correlation is 0.053, and the maximum error within 8.3%.

To highlight the effect of thermal Grashof number on both average Nusselt and Sherwood numbers, the thermal Grashof number was varied from 2×10^3 to 5×10^6. The Lewis number was kept constant at *Le*=1, buoyancy ratio N=1, and inclination angle φ=10. The results are plotted in fig. 12. In general, the average Nusselt increases with the thermal Grashof number. A sudden drop in the value of *Nu* occurs at Gr_T=4×10^5. To explore the reason of this drop, the streamlines for Gr_T=4×10^5 and for Gr_T=6×10^5 are plotted in fig. 13. The figure shows transition in the flow from four pair of cells at Gr_T=4×10^5 to two pair of cells at Gr_T=6×10^5. This transitions in flow drops the rate of heat and mass transfer.

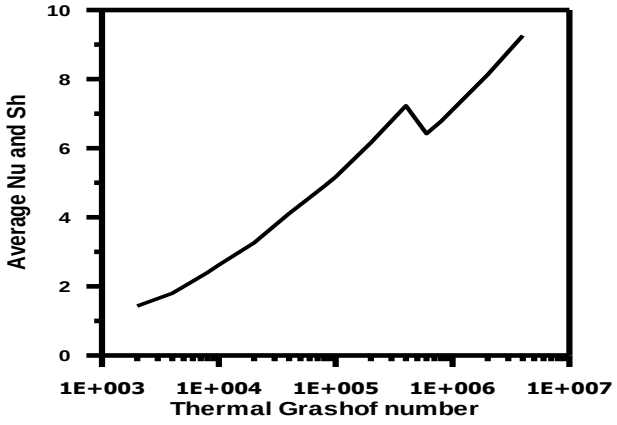

Fig. 12 Effect of thermal Grashof number on both Average Nusselt and Sherwood numbers, *Le*=1, N=1 andφ=10°.

$Gr_T=4x10^5$ $Gr_T=6x10^5$

Fig. 13. Streamlines *Le*=1, N=1 and φ=10°.

5. Comparison of the nusselt number results

A comparison of the present results for Nusselt with those published by Lam et al. [13], and Boussaid et al. [21] was made.

5.1. Comparison

A comparison was made at with Lam et al. [13] three values of φ equals 5°, 10°, and 15°. As illustrated in table 1, there is a wide agreement of data between Lam experimental results and the present result for φ=5°. The present result is less than Lam's result by about 4.9%. But for φ =15°, there is a departure in the curve obtained by Lam. The deviation reached approximately 12.48% as shown in the table. Lam correlated his experimental results in the following correlation:-

$$Nu = 0.168\left[Ra_T\left(\frac{1+\cos\varphi}{2}\right)\right]^{0.278} \times \left[\frac{1-\cos\varphi_{\max}}{\cos\varphi-\cos\varphi_{\max}}\right]^{-0.199}. \quad (20)$$

As shown in fig. 14, there is a big deviation between the experimental results of Lam, and the results obtained from his correlation. The average *Nu* obtained from the correlation is lower than those obtained from experimental results. The deviation between the two results is about 18% for φ=5°, and 21% for φ =15°.

Table 1
Comparison with Lam et al. [13]

φ(Degree)	5	10	15
Nu(Lam experimental results)	4.5	4.3	3.8
Nu(Lam eqn.)	3.676	3.475	2.99
%Deviation between lam results and lam equation	18.31	19.17	21.31
Nu(Present work)	4.29	4.35	4.36
%Deviation between present work and Lam experimental results	-4.899	1.15	12.84

Some of the obtained results were compared with the results published by Boussaid [21]. The comparison was made at two values of φ= 5°, and 10°. Fig. 14 shows the comparison at Gr_T = 10^5, A = 3, and different inclination angle (φ). As shown from figure, there is a departure in the result obtained by Boussaid. The deviation reached approximately 12% as shown in the fourth row of table 2. As the inclination angle φ, is increased to 10°, a wide agreement can be found with deviation of approximately 5% as shown in table 2.

6. Conclusions

The laminar natural heat and mass transfer in a symmetrical trapezoidal enclosure with vertical temperature and concentration gradients has been studied numerically for both aiding and opposing buoyancy forces. The bottom and ceiling are considered isothermal

Table 2
Comparison with Boussaid et al. [21]

φ (Degree)	5	10
Nu (Boussaid)	3.86	4.6
Nu (Present work)	4.29	4.368
%Deviation	10.023	-5.31

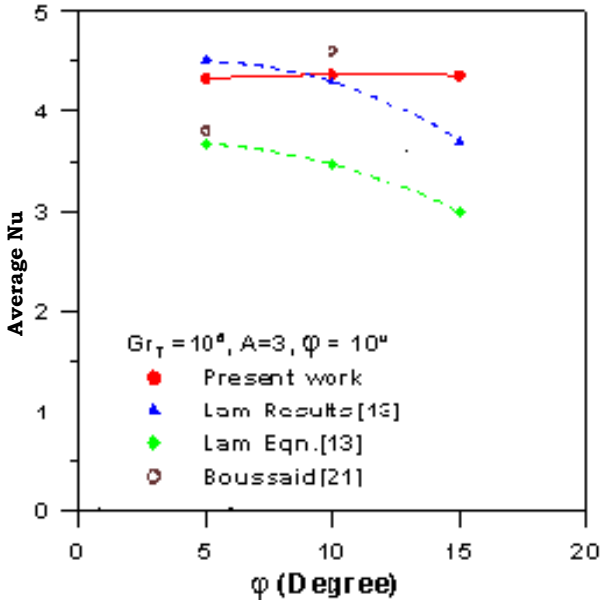

Fig. 14. Comparison of average *Nu* results for A=3, φ=10°, and Gr_T=10^5 when *Le*=1.

and isoconcentration surfaces, while the vertical walls are assumed adiabatic and impermeable surfaces The investigation is made for wide range of buoyancy ratio N, $-1 \le N \le 10$, ceiling inclination angle φ, $0^o \le \varphi \le 18.44^o$, (the two extremes 0^o for rectangular cavity and 18.44^o for triangle cavity) and Lewis number Le, $1 \le Le \le 5$ with fixed aspect ratio A, at A=3, and thermal Grashof number $Gr_T = 10^5$. The main investigation is made when $\varphi = 10^o$. The following remarks were concluded.

1. For Lewis number equals one the isothermal and isoconcentration lines are congruent and both average Nusselt number and average Sherwood number are equal.
2. Multy cells were observed in the stream lines, these cells were strong in the middle of the cavity and weak near the cavity wall.
3. The local Nusselt and local Sherwood numbers look like the saw tooth distribution over the cavity base.
4. The Lewis number has a minor effects on the average Nusselt number. The Nusselt number is slightly decreased as the Lewis is increased.
5. The buoyancy ratio has a major effect on the average Nusselt and Sherwood numbers. They are increased as the buoyancy ratio is increased.
6. The average Nusselt and Sherwood numbers are slightly increased as the ceiling inclination angle is increased.
7. A transition of the flow field from four cells to three cells and then to two cells occurred as both *Le*, and N is increased. A rapid decreasing in both average *Nu* and average *Sh* is noticed when the transition of flow field occurred. As inclination angle is increased, both average *Nu* and average Sh are increased.

Both Nusselt number and Sherwood number can be correlated as follows:

$$Nu = 6.358 N^{0.0294} Le^{-0.188}$$

$$Sh = 6.561 N^{0.0227} Le^{0.1303}$$

Nomenclature

A is the aspect ratio, L/H_o
c is the vapour concentration
C is the dimensionless vapour concentration, $C=(c-c_i)/(c_o-c_i)$
c_o, c_i is the concentrations at the bottom, and the ceiling of the cavity, respectively
D is the mass diffusivity, m^2/s
g is the acceleration of gravity, m/s^2
Gr_S is the solutal Grashof number based on the half width of the cavity, $Gr_S = g\beta(c_i - c_o)H_o^3/\gamma^2$
Gr_T is the thermal Grashof number based on the half width of the cavity, $Gr_T = g\beta(T_i - T_o)H_o^3/\gamma^2$
h is the heat transfer coefficient , W/m^2K
h_s is the solutal transfer coefficient, m/s
H_o is the maximum height of the cavity, m
k is the fluid thermal conductivity, W/m K
L is the half cavity width, m
Le is the Lewis number, $Le = \alpha/D = Sc/Pr$
N is the Buoyancy ratio, $N = \beta_S \Delta C / \beta \Delta T$, or $N = Ra_S/Ra_T$
Nu is the average Nusselt number, $Nu = \dfrac{hH_o}{k}$.
Nu_i is the local Nusselt number, $Nu_i = -\left(\dfrac{\partial \theta}{\partial Y}\right)_{Y=0}$
p is the pressure, N/m^2
P is the dimensionless pressure, $P = pH_o^2/\rho_o \alpha^2$
Pr is the Prandtl number, $Pr = \gamma/\alpha$
Ra_S is the solutal Rayleigh number, $Ra_S = Gr_S * Pr$
Ra_T is the thermal Rayleigh number, $Ra_T = Gr_T * Pr$
Sc is the Schmidt number, $Sc = \gamma/D$
Sh is the Average Sherwood number, $Sh = \dfrac{h_S H_o}{D}$
Sh_i is the local Sherwood number, $Sh_i = -\left(\dfrac{\partial C}{\partial Y}\right)_{Y=0}$
T is the local temperature, K
T_o, T_i is the temperatures at the bottom and upper cavity surfaces respectively, K
ΔT is the temperature difference, $(T_o - T_i)$, K
u , v is the velocity components in the x and y directions respectively, m/s
U , V is the dimensionless velocity components in the X and Y directions respectively, ($U = uH_o/\alpha$ and $V = vH_o/\alpha$)
x, y is the dimensional coordinates, m and
X,Y is the dimensionless coordinates, $X = x/H_o$ and $Y = y/H_o$.

Greek symbols

β_T is the coefficient of thermal expansion, K^{-1}
β_S is the coefficient of solutal expansion, kg^{-1}
α is the thermal diffusivity, m^2/s
θ is the dimensionless temperature, $(T - T_i) / (T_o - T_i)$
γ is the kinematic viscosity, m^2/s
ρ is the local fluid density, kg/m^3
ρ_o is the fluid density at the bottom surfaces, kg/m^3
φ is the angle of inclination, and
μ is the dynamic viscosity, kg/m.s.

References

[1] C.Y. Hu, M. M. EL-Wakil, "Simultaneous Heat and Mass Transfer in a Rectangular Cavity", Proc. 5th Int. Heat Transfer Conf. Vol. 5, pp. 24-28 (1974).

[2] S. Ostrach, "Natural Convection with Combined Driving Forces", Physico Chem Hydrdyn 1, pp. 233-247 (1980).

[3] S. Ostrach, "Natural Convection Heat Transfer in Cavities and Cells", 7th Int. Heat Transfer Conf., Munich, 1982, Vol. 1, pp. 365-379 (1983).

[4] S. Ostrach, Fluid Mechanics in Crystal Growth-the 1982 Freeman Scholar Lecture, J. Fluid Eng. 105, pp. 5-20 (1983).

[5] T.S. Lee, P.G. Parikh, A. Acrivos, and D. Bershader, "Natural Convection in a Vertical Channel with Opposing Buoyancy Forces", Int. J. Heat and Mass Transfer, 25, pp. 499-511 (1982).

[6] S. Kimura, and A. Bejan, "The Boundary Layer Natural Convection Regime in a Rectangular Cavity with Uniform Heat Flux from the Side", ASME J. Heat Transfer 106, pp. 98-103 (1984).

[7] O.V. Trevisan, and A. Bejan, "Combined Heat and Mass Transfer by Natural Convection in a Vertical Enclosure", ASME J. Heat Transfer 109, pp. 104-112 (1987).

[8] P. Ranganathan, and R. Viskanta, "Natural Convection in a Square Cavity Due to Combined Driving Forces", J. Numerical Heat Transfer 14, pp. 35-59 (1986).

[9] C. Beghein, F. Haghighat and F. Allard, "Numerical Study of Double-Diffusive Natural Convection in a Square Cavity", Int. J. Heat and Mass Transfer 35, pp. 833-846 (1992).

[10] H. Han and T.H. Kuehn, "Double Diffusive Natural Convection in a Vertical Rectangular Enclosure – I- Experimental Study", Int. J. Heat and Mass Transfer 34, pp. 449-459 (1991).

[11] H. Han and T.H. Kuehn, "Double Diffusive Natural Convection in a Vertical Rectangular Enclosure – II- Numerical Study", Int. J. Heat and Mass Transfer 34, pp. 461-471 (1991).

[12] D. Poulikakos. A. Be-Jan., "The Fluid Dynamics of an Attic Space", J. Fluid Mech. 131 pp. 251-269 (1983).

[13] S.W. Lam, R. Gani and J.O. Symons, "Experimental and Numerical Studies of Natural Convection in Trapezoidal Cavities", ASME J. Heat Transfer 111, pp. 372-377 (1989).

[14] T.S. Lee, "Numerical Experiment with Fluid Convection in Tilted Nonrectangular Enclosures", Numerical Heat Transfer, Part A 19 (4) pp. 487-499 (1991).

[15] H. Salmun, "Convection Patterns in a Triangular Domain", Int. J. Heat and Mass Transfer
Vol. 38 (2), pp. 351-361 (1995).

[16] K. Voropoulos, E. Mathioulakis and V. Bekssiotis, "Transport Phenomena and Dynamic Modeling in Greenhouse-Type Solar Stills", Desalination 129 (3) pp. 273-281 (2000).

[17] J. Rheinllnder, "Numerical Calculation of Heat and Mass Transfer in Solar Stills", Solar Energy 28 (2), pp. 173-179 (1982).

[18] A. Palacio, J.L. Fernandez, "Numerical Analysis of Greenhouse-Type Solar Stub with High Inclination", Solar Energy 50 (6), pp. 469-476 (1993).

[19] B. Djebedjian and M. Abou Rayan, "Theoretical Investigation on the Performance Prediction of Solar Still", Desalination 128 (2), pp. 139-145 (2000).

[20] E. Papanicolaou, K. Voropoulos and V. Belessiotis, "Natural Convective Heat Transfer in an Asymmetric, Greenhouse-Type Solar Still—Effect of Angle of Inclination", Numerical Heat Transfer. Part A 42 (8), pp. 855-880 (2002).

[21] M. Boussaid. A. Djerrada and M. Bouhadef, "Thermosolutal Transfer within

Trapezoidal Cavity", Num. Heat Transfer. Part A 43 (4), pp. 431-448 (2003).
[22] K. Ghorayeb and A. Mojtabi, "Double Diffusive Convection in a Vertical Rectangular Cavity", Phys-Fluid 9 (8), pp. 2339-2348 (1997).
[23] K. Ghorayeb, H. Khallouf and A. Mojtabi, "Onset of Oscillatory Flows in Double-Diffusive Convection", Int. J. Heat and Mass Transfer 42 (4), pp. 629-643 (1999).
[24] M. Mamou, P. Vasseur and M. Hasnaoui, "On Numerical Stability Analysis of Double-Diffusive Convection in Confined Enclosures", J. Fluid Mech. 433, pp. 209-250 (2001).
[25] E. Papanicolaou and V. Belessiotis, "Double-Diffusive Natural Convection in an Asymmetric Trapezoidal Enclosure: Unsteady Behavior in the Laminar and the Turbulent-Flow Regime", Int. J. Heat and Mass Transfer 48, pp. 191-209 (2005).
[26] S.V. Patankar, "Numerical Heat Transfer and Fluid Flow", McGraw-Hill, New York (1980).

Received April 15, 2006
Accepted May 27, 2006